

Supporting Information for

Stable Ferromagnetism and Half-metallicity in Two-Dimensional  
Polyporphyrin Frameworks

Jie Tan,<sup>a</sup> Weifeng Li,<sup>b</sup> Xiujie He,<sup>a</sup> Mingwen Zhao<sup>a,\*</sup>

<sup>a</sup> *School of Physics and State Key Laboratory of Crystal Materials, Shandong University, Jinan 250100, Shandong, China. E-mail: zmw@sdu.edu.cn*

<sup>b</sup> *School of Biological Sciences, Nanyang Technological University, 60 Nanyang Drive, Singapore, 637551*

Contents:

1. Isomeric patterns for 2D periodic 2H-PP frameworks.
2. Electronic structures of 2D metal-free PP sheets.
3. Spin-resolved electron density of states of 2D TM-PP frameworks.
4. The band structures of Cr-PP systems with different electron doping rates.

## 1. Isomeric patterns for 2D periodic metal-free PP frameworks.

To search for the energetically most favorable hydrogenating pattern, we employed a large supercell containing four aromatic rings. There are four hydrogenating patterns for this supercell which are labeled as AAAA, AAAB, ABAB, and ABBA, as shown in Figure S1. The primitive cells of these patterns are represented by the rectangles and squares with dashed borderlines. The total energies of these patterns relative to the energetically most stable pattern are listed in table S1. Electron spin-polarization effects were taken into account in these calculations. It is clear that the ABBA pattern is energetically most stable among the four patterns considered in this work.

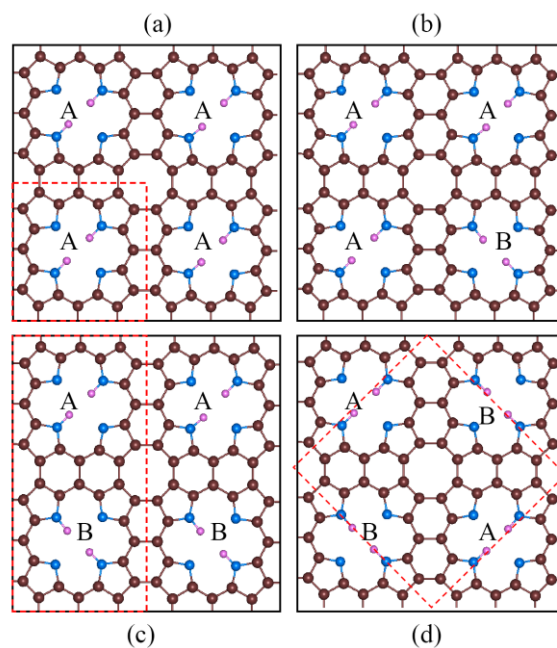


**Fig. S1.** Four isomeric patterns for 2D periodic 2H-PP frameworks.

**Table S1.** Total energies of different patterns relative to the energetically most favorable pattern.

	AAAA	AAAB	AABB	ABBA
$\Delta E$ (eV)	0.481	0.225	0.192	0.000

## 2. Electronic structures of 2D metal-free PP sheets

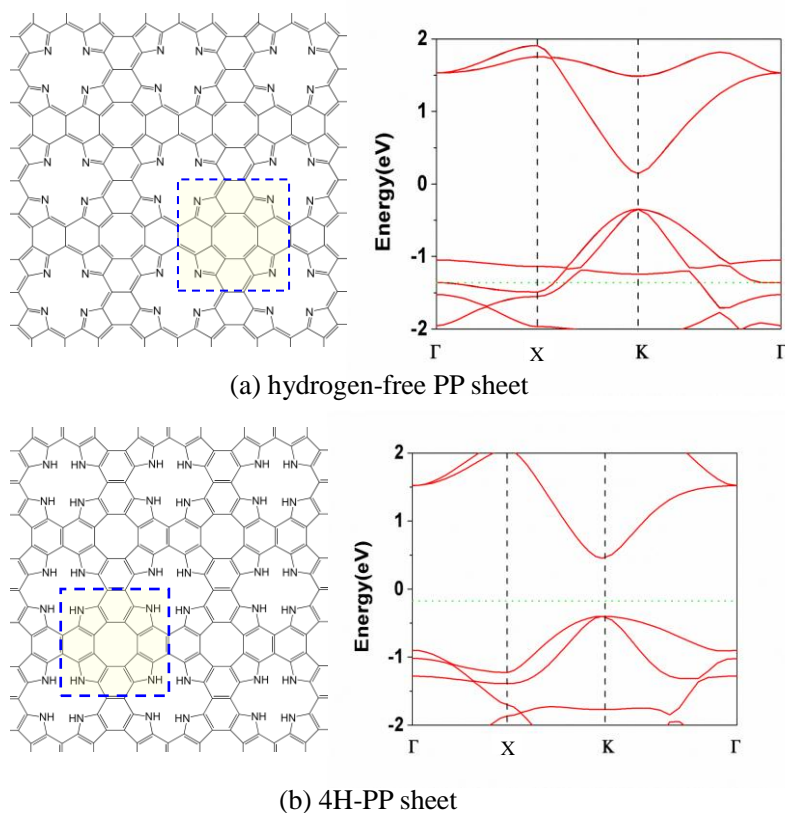


**Fig. S2.** The geometric and electronic structures of metal-free PP sheets. The squares with dashed borderlines represent the primitive cells of these 2D periodic sheets. The dashed lines in the right panel indicate the position of the Fermi level.

We designed the two metal-free PP sheets with equivalent COT-based units by removing all the H atoms (hydrogen-free PP sheet) or introducing more H atoms to saturate all the N atoms in pyrroles (4H-PP sheet). The Lewis structures of these two configurations are shown in the left panel of Figure S2. The band structures shown in the right panel of Figure S2 indicate that the electrons of these two configurations are spin compensated. Hydrogen-free PP sheet is metallic with two dispersed bands across the Fermi level. The electronic states at the Fermi level are rather dispersive, implying that hydrogen-free PP is not in a radical state. This is due to the redistribution of the unpaired electrons of N atoms. However, it is noteworthy that hydrogen-free PP has a strong tendency to get two electrons because the total energy calculations indicate that its -2 charge state is energetically most favorable.

Therefore, when transition metal atoms are incorporated into hydrogen-free PP, electron transfer from metal atoms to PP sheet takes place and the metal atoms are at +2 charge state. The whole system remains neutral. 4H-PP is semiconducting with a direct band gap of 0.76 eV at the K(1/2, 1/2, 0) point. We also employed a hybrid functional (HSE functional) to calculate the band gap of 4H-PP sheet, and found that it is 1.25 eV. This band gap is comparable to that of silicon crystal, suggesting the potential application of 4H-PP sheet in solar cells.

### 3. Spin-resolved electron density of states of 2D TM-PP frameworks.

**Table S2.** The electron occupation (EO) of the d orbitals and the corresponding magnetic moments (MM) of TM-PP frameworks. The values from first-principles calculations (cal.) are also presented for comparison. The differences between the model and first-principles calculations arise from the contributions of the polyporphyrin sheet to the magnetic moments which are not taken into account in the model.

	Mn-PP	Ni-PP	Fe-PP
EO	$(d_{xy}^{\uparrow})^1(d_{\pi}^{\uparrow})^2(d_{z^2}^{\uparrow})^1$	$(d_{xy}^{\uparrow\downarrow})^2(d_{\pi}^{\uparrow\downarrow})^4(d_{z^2}^{\uparrow\downarrow})^2$	$(d_{\pi}^{\uparrow})^2(d_{\pi}^{\uparrow})^1(d_{z^2}^{\uparrow})^1(d_{xy}^{\uparrow\downarrow})^2$
MM(model)	4	0	2
MM(cal.)	3.8	0	2
	Cu-PP	Zn-PP	
EO	$(d_{\pi}^{\uparrow\downarrow})^4(d_{z^2}^{\uparrow\downarrow})^2(d_{xy}^{\uparrow\downarrow})^2(d_{x^2-y^2}^{\downarrow})^1$	$(d_{\pi}^{\uparrow\downarrow})^4(d_{z^2}^{\uparrow\downarrow})^2(d_{xy}^{\uparrow\downarrow})^2(d_{x^2-y^2}^{\downarrow})^2$	
MM(model)	1	0	
MM(cal.)	1.4	0	

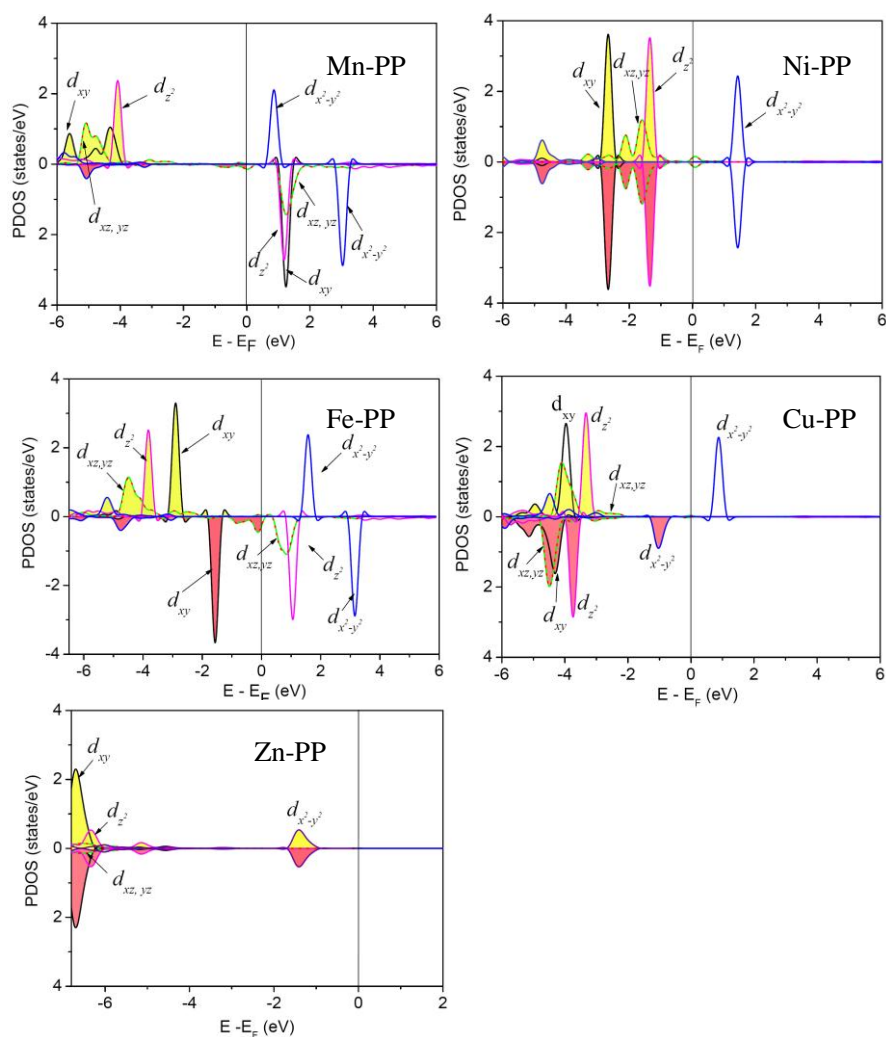


**Fig. S3.** Spin-resolve electron density of states projected onto the TM (TM=Mn, Ni, Fe, Cu, and Zn) atoms of 2D periodic TM-PP frameworks. Spin-up and spin-down branches are plotted in the up and down panels, respectively. The energy at the Fermi level was set to zero.

4. The band structures of Cr-PP systems with different electron doping rates.

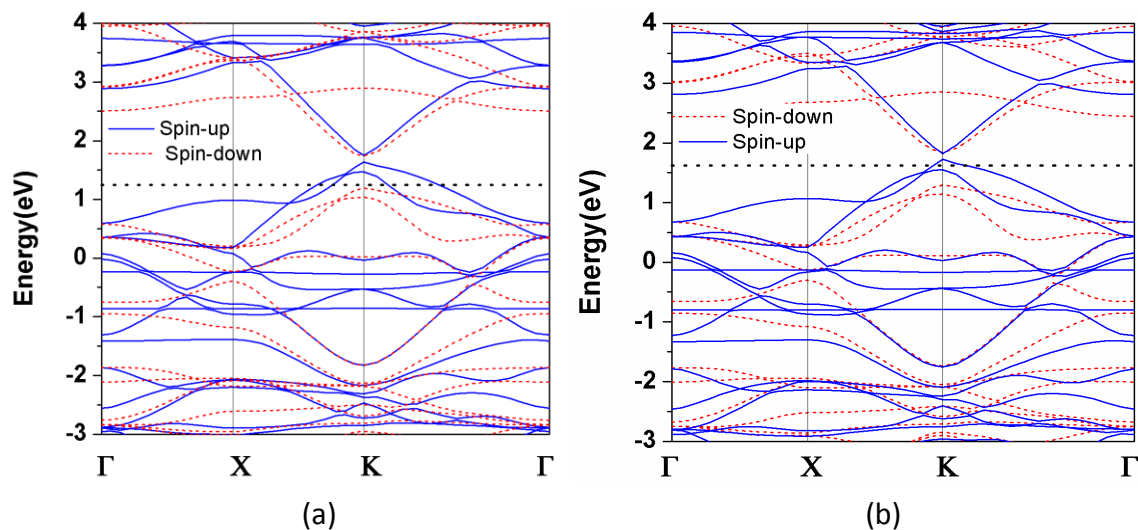


Fig. S4. Spin-resolved band structures of Cr-PP structure with different electron doping rates

The position of Fermi level can be tuned by electron doping. We therefore calculated the band structures of Cr-PP with different electron doping rates to mimic such effect. Our calculations indicate that when the electron doping rate is 15%~18%, the Fermi level just falls in the gray strip and half-metallicity can be achieved in Cr-PP sheet